4-13-2015

Accelerated glacier melt on Snow Dome, Mount Olympus, Washington, USA, due to deposition of black carbon and mineral dust from wildfire

Susan D. Kaspari

S. McKenzie Skiles

Ian Delaney

Daniel Dixon

Thomas H. Painter

AGU PUBLICATIONS

JGR

Journal of Geophysical Research: Atmospheres

RESEARCH ARTICLE
10.1002/2014JD022676

Key Points:
- Impurity deposition on Snow Dome was a magnitude higher postfire
- The higher impurity deposition reduced albedo and increased melt
- River discharge increased at the time of the impurity deposition

Correspondence to:
S. Kaspari,
kaspari@geology.cwu.edu

Citation:
Kaspari, S., S. McKenzie Skiles, I. Delaney, D. Dixon, and T. H. Painter (2015), Accelerated glacier melt on Snow Dome, Mount Olympus, Washington, USA, due to deposition of black carbon and mineral dust from wildfire, *J. Geophys. Res. Atmos.*, *120*, 2793–2807, doi:10.1002/2014JD022676.

Received 6 OCT 2014
Accepted 10 MAR 2015
Accepted article online 13 MAR 2015
Published online 13 APR 2015

Accelerated glacier melt on Snow Dome, Mount Olympus, Washington, USA, due to deposition of black carbon and mineral dust from wildfire

Susan Kaspari[1], S. McKenzie Skiles[2], Ian Delaney[1], Daniel Dixon[3], and Thomas H. Painter[4]

[1]Department of Geological Sciences, Central Washington University, Ellensburg, Washington, USA, [2]Joint Institute for Regional Earth System Science and Engineering, University of California, Los Angeles, California, USA, [3]Climate Change Institute, University of Maine, Orono, Maine, USA, [4]Jet Propulsion Laboratory, California Institute of Technology, Pasadena, California, USA

Abstract Assessing the potential for black carbon (BC) and dust deposition to reduce albedo and accelerate glacier melt is of interest in Washington because snow and glacier melt are an important source of water resources, and glaciers are retreating. In August 2012 on Snow Dome, Mount Olympus, Washington, we measured snow surface spectral albedo and collected surface snow samples and a 7 m ice core. The snow and ice samples were analyzed for iron (Fe, used as a dust proxy) via inductively coupled plasma sector field mass spectrometry, total impurity content gravimetrically, BC using a single-particle soot photometer (SP2), and charcoal through microscopy. In the 2012 summer surface snow, BC (54 ± 50 μg/L), Fe (367±236 μg/L) and gravimetric impurity (35 ± 18 mg/L) concentrations were spatially variable, and measured broadband albedo varied between 0.67–0.74. BC and dust concentrations in the ice core 2011 summer horizon were a magnitude higher (BC = 3120 μg/L, Fe = 22000 μg/L, and gravimetric impurity = 1870 mg/L), corresponding to a modeled broadband albedo of 0.45 based on the measured BC and gravimetric impurity concentrations. The Big Hump forest fire is the likely source for the higher concentrations. Modeling constrained by measurements indicates that the all-sky 12 h daily mean radiative forcings in summer 2012 and 2011 range between 37–53 W m^{-2} and 112–149 W m^{-2}, respectively, with the greater forcings in 2011 corresponding to a 29–38 mm/d enhancement in snowmelt. The timing of the forest fire impurity deposition is coincident with an increase in observed discharge in the Hoh River, highlighting the potential for BC and dust deposition on glaciers from forest fires to accelerate melt.

1. Introduction

Washington State has the largest concentration of glaciers in the contiguous United States. Meltwater from these glaciers provides an important source of water resources, accounting for nearly 50% of the May–September runoff in some watersheds. Glacier melt is variable from year to year, with glacier melt contributing a greater amount of water during years when the snowpack is minimal. Glacier melt thus provides a source of water resources that can act as a buffer during drought years [*Riedel and Larrabee*, 2011].

As in most alpine regions, glaciers in Washington State are retreating [*Riedel and Larrabee*, 2011]. While increasing temperatures and reductions in snow accumulation are well-recognized factors contributing to glacier retreat [*McCabe and Fountain*, 2013; *Rasmussen et al.*, 2000], another cause is the deposition of light absorbing impurities (LAI) onto snow and glacier surfaces [*Painter et al.*, 2013a]. Snow has the highest albedo of any naturally occurring surface on Earth. When LAI are present, the snow albedo decreases, resulting in greater absorption of solar energy and accelerated snow and ice melt [*Conway et al.*, 1996; *Warren and Wiscombe*, 1980].

LAI include black carbon (BC, a dark absorptive particle produced by the incomplete combustion of biomass and fossil fuels), brown carbon (light-absorbing organic matter), and dust. These impurities have a short residence time in the atmosphere (days to weeks), resulting in regional variations in LAI concentrations in the atmosphere and snow/ice. BC emissions have increased globally in recent decades, but emission trends vary regionally [*Bond et al.*, 2007]. In the Pacific Northwest sources of BC include the transportation sector, residential biofuel combustion (primarily wood burning stoves for heating), forest fires, and potentially long-range transport from Asia [*Bond et al.*, 2004]. Dust originates from both natural and anthropogenic sources, with anthropogenic emissions associated with agriculture, deforestation, and other changes in land use [*Tegen et al.*, 2004].

The role of LAI in accelerating snow and glacier melt is an emerging research topic, and few studies have taken place investigating the impacts of LAI on snow and ice melt in the Pacific Northwest. *Grenfell et al*. [1981] measured LAI in a snowpack in the Cascade Mountains and determined that LAI reduced the albedo, while *Clarke and Noone* [1985] provided measurements of BC concentrations in old and new surface snow samples from the Olympic peninsula. *Conway et al*. [1996] applied manufactured BC on the snowpack at Snow Dome on Blue Glacier in the Olympic Mountains and found that BC applied in high enough concentrations to cause a 30% reduction in albedo-increased melting by 50%. More recently, *Delaney* [2013] measured BC in the seasonal snowpack at Blewett Pass in Central Washington from 2010 to 2013 and on glaciers around Washington State in 2012, and found that BC increased over the spring-summer from its low in the winter snowpack. The higher concentrations during the summer were attributed to increased dry deposition associated with the seasonal increase in the planetary boundary layer height and minimal precipitation. Additionally, in 2012 the Table Mountain wildfire burned the forest surrounding the Blewett Pass seasonal snow study site. In the following winter, BC deposited in the snowpack was at least fourfold higher than prefire, with charred snags the presumed source of the elevated BC.

Forest fires are increasingly recognized as having an effect on snow and glacier melt. In forested areas, snow accumulation and ablation are affected postfire by a reduction in canopy interception, which increases light transmission, alters the surface energy balance, and accelerates snowmelt [*Burles and Boon*, 2011; *Harpold et al*., 2014]. In addition to changes in the forest canopy, *Gleason et al*. [2013] demonstrated that pyrogenic carbon particles and burned woody debris shed from standing charred trees reduce snow albedo, resulting in earlier melt out of the seasonal snowpack. Furthermore, because emissions from forest fires can be transported long distances, forest fires can have far-reaching impacts beyond forested regions. *Keegan et al*. [2014] recently linked widespread melt of the Greenland ice sheet to Northern Hemisphere forest fires. The impacts of forest fire on snow and glacier melt are of concern, as wildfire frequency, size, intensity and duration are increasing across the western U.S. [*Westerling et al*., 2006], and this trend is expected to continue. In Washington State, the area burned by fire is projected to double by the 2040s and triple by the 2080s [*Littell et al*., 2009]. Despite the linkage between forest fires and snow and glacier melt, little research has been conducted investigating LAI-induced melt from forest fires [*Keegan et al*., 2014].

We present the results of a study investigating LAI concentrations in snow and ice conducted on Snow Dome on the Blue Glacier of Mount Olympus in northwestern Washington (Figure 1). This site was targeted to further characterize LAI deposition on glaciers in Washington State, and was initially of interest because it is located predominantly upwind of major urban areas, and was thus hypothesized to represent background LAI concentrations in snow and ice in the Pacific Northwest region. However, we observed markedly higher BC and dust concentrations than previously observed in the region that we attribute to forest fire. Herein, we examine the effects of LAI deposition on radiative forcing and accelerated melt on Snow Dome.

2. Methods

2.1. Site Description

Fieldwork was conducted in August 2012 on Snow Dome on the Blue Glacier, Mount Olympus (47.815°N, 123.702°W, 2080 m) in Washington State, USA (Figure 1). Blue Glacier is a temperate glacier with an elevation range of 1275–2350 m, and an area of 4.3 km^2. While mass balance on the Blue Glacier has been negative since the 1970s, the mass loss is less than on other glaciers in the region [*Conway et al*., 1999]. Blue glacier has been the focus of numerous glaciology studies since the 1950s [e.g., *Conway et al*., 1999; *LaChapelle*, 1959; *Rasmussen et al*., 2000]. The majority of the snowfall on Blue Glacier occurs between October and May (winter snow accumulation can be in excess of 10 m depth), with the moisture flux coming from the southwest associated with extratropical cyclones [*Rasmussen et al*., 2000; *Waddington and Marriot*, 1986].

2.2. Field Methods

A 7.8 m snow/ice core was collected on Snow Dome using a solar powered 5 cm electromechanical ice core drill (icedrill.ch). Surface snow samples from sites spatially distributed on Snow Dome (Figure 1) were collected from the upper 3 cm of the snowpack and stored in 50 mL polypropylene vials or Whirlpak bags. Polypropylene gloves were worn at all times during sample collection. Snow and ice samples were removed from the glacier by helicopter and maintained frozen until analysis.

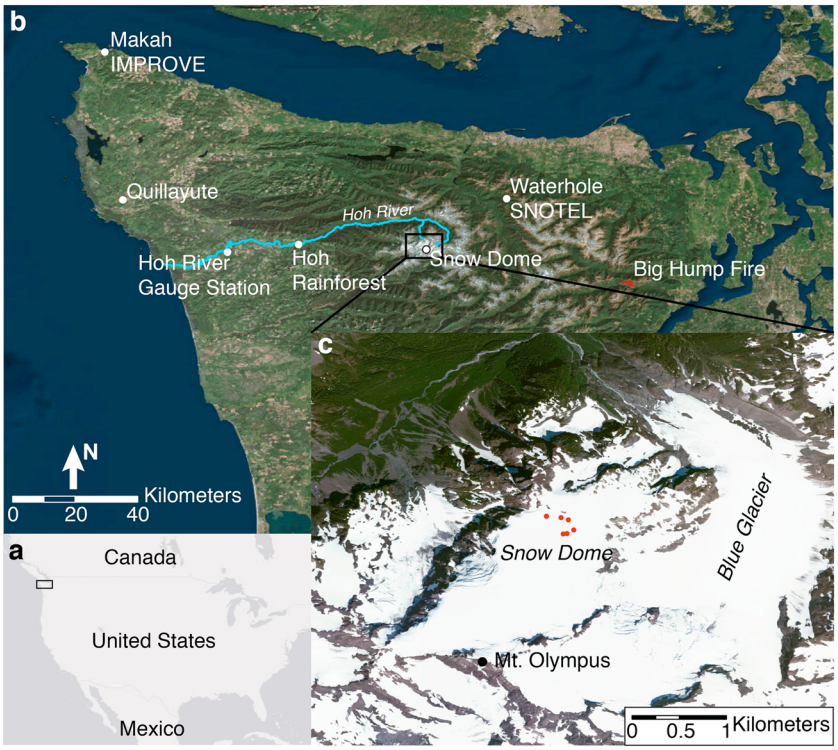

Figure 1. Location map showing (a) the Olympic Peninsula in Washington State, USA; (b) Snow Dome, the Hoh River, and the location of instrumental data used in the study and the Big Hump forest fire, and (c) Snow Dome, the Blue Glacier, and Mount Olympus. Sampling sites are indicated by red circles.

Spectral albedo was measured using an Analytical Spectral Devices (ASD) FieldSpec3 spectrometer and a tripod mounted cosine receptor at the sites where surface snow samples were collected. Albedo is the average of 10 up-looking and 10 down-looking measurements. Up-looking spectra are collected by placing the tripod on a flat plate plane parallel to the snow surface, while down-looking spectra are collected by holding the tripod with the cosine receptor parallel to the snow surface. The spectrometer contiguously samples the spectral region between 0.35 and 2.5 μm, with a spectral resolution ranging from 0.003 μm (at 0.7 μm) to 0.01 μm (at 1.4 and 2.1 μm). Some uncertainty can be introduced into the measurement when the down-looking collections are done by hand, as it can be difficult to keep the cosine receptor perfectly level and at the same distance from the snow surface. However, the sensitivity of albedo to this method was fairly low for these measurements, with the broadband albedo from the 10 measurements at each site exhibiting a variance of ±0.0002 and differing by no more than ±0.03 from the average (reported) broadband albedo at each site. A problem with the spectrometer shortwave infrared (SWIR) 2 detector produced noise in the signal across the detectors spectral range (between 1.8 and 2.5 μm), and here we limit the wavelength range used to 0.35 to 1.8 μm. There is little information lost through this restriction, as the majority of irradiance and snow reflectance occurs between 0.35 and 1.8 μm [*Wiscombe and Warren*, 1980].

2.3. Laboratory Methods

In the laboratory, the ice core was sampled at 3–10 cm depth resolution, and the outer section of the core was removed using a ceramic knife and an ice core lathe. The inner section of the core was placed in precleaned polypropylene vials.

Ice core and snow samples were melted just prior to BC analysis. The samples were sonicated for 20 min and stirred with a magnetic stirrer during analysis. The liquid samples were pumped using a peristaltic pump, nebulized using a CETAC U-5000 AT^{+} ultrasonic nebulizer, and the resultant dry aerosol was coupled to the sample inlet on a single-particle soot photometer (SP2). The SP2 uses laser-induced incandescence to determine the mass of refractory BC in individual particles [*Schwarz et al.*, 2006]. Monitoring of liquid

sample flow rate pumped into the nebulizer, fraction of liquid sample nebulized and purge airflow rate allows BC mass concentrations in the liquid sample to be determined. Because BC is not nebulized with 100% efficiency, Aquadag standards were used to correct the measured BC concentrations for BC losses that occur during nebulization [*Wendl et al*., 2014]. The BC concentrations reported herein predominantly represent the mass of BC particles 500 nm diameter and smaller, which corresponds to the size range where the mass absorption cross section of BC particles is greater relative to larger particles, meaning that smaller BC particles absorb light and reduce albedo more efficiently [*Schwarz et al*., 2013]. *Wendl et al*. [2014] and *Kaspari et al*. [2014] provide further details on the SP2 analytical method.

After samples were analyzed for BC, an aliquot was removed from each vial for trace element analysis. Samples for trace element analysis were acidified to 1% HNO_3 using double distilled HNO_3 and allowed to react with the acid for 2 weeks before being refrozen. Trace element analysis was conducted at the Climate Change Institute, University of Maine, using a Thermo Electron Element2 inductively coupled plasma sector field mass spectrometer (ICP-SFMS) [*Osterberg et al*., 2006].

The total impurity load in select samples was determined gravimetrically. Melted snow samples (250–600 g for surface samples; 5 g for ice core samples) were filtered through a preweighed 0.45 μm Millipore filter (HAWP02400) using a vacuum pump and dried overnight in a laminar flow hood. The dry mass on the filter reflects the impurity mass of the sample larger than 0.45 μm, with dust assumed to contribute the majority of the dry mass [*Kaspari et al*., 2014]. Organic matter on the same filters was identified via epifluorescence at Miami University using a Nikon LV100 compound microscope with an Intensilight C-HGFI Illumination unit (Endow GFP longpass green filter: exciter HQ470/40 ex, dichroic 495, and emitter 500LP). This filter was chosen because it transmits wavelengths that are ideal for exciting plant organic matter. Photographs were taken with a Nikon Digital Sight DS-Ri1 camera and NIS-Elements v. 3.22.11 with extended depth of focus capabilities. Plant-derived organic matter was limited to pollen from the surrounding forest, and qualitative assessment confirms that the impurity mass was strongly dust dominated. That dust dominates impurity mass is consistent with *Takeuchi* [2002, 2009], who reported that organic matter contributes 3–13% of impurity mass. Herein, we treat the total impurity load as dust.

Select samples from the ice core were processed for microscopic charcoal analysis in the Paleoecology Lab at Central Washington University following the methods reported by *Eichler et al*. [2011]. The samples were placed in 50 mL centrifuge tubes and centrifuged at 3500 rpm for 3 min. The liquid was decanted from the sample vial, silicon oil was added as a mounting medium, and the sample was mixed using a vortex mixer. Using a pipette, the sample was mounted on a slide and examined for the presence of charcoal using a compound microscope at 400X magnification.

Hemispherical reflectance of filtered impurities from the 2011 and 2012 summer horizons was measured between 0.35 and 2.5 μm wavelength with an ASD RTS-3ZC integrating sphere coupled to an ASD FieldSpec3 spectrometer at the Snow Optics Laboratory at NASA's Jet Propulsion Laboratory [*Skiles*, 2014]. The integrating sphere has a collimated tungsten light source that delivers close to solar irradiance level light, and an internal coating of Zenith® diffuse polymer material that is a Lambertian reflector over the instrument's spectral range that ensures retrievals are insensitive to directional reflectance features coming from the sample. Reported reflectance is the ratio between the measured reflectance from the sample and that from the Zenith® diffuse reference standard. The samples were visually optically thick, but due to the possibility of light transmission through the sample and reflectance from the sample filter, the retrievals are used here simply as a relative comparison of impurity layer reflectance.

2.4. Modeling

The SNow, ICe, and Aerosol Radiation (SNICAR) model was used to compute the snow spectral albedo [*Flanner and Zender*, 2005, 2006] for no impurities (clean snow) and snow containing BC and dust (observed snow). SNICAR simulates radiative transfer in the snowpack utilizing theory from *Warren and Wiscombe* [1980], which uses Mie theory to calculate single scattering by snow particles and the delta-Eddington approximation [*Joseph et al*., 1976] for multiple scattering of solar radiation in the snowpack, and the two stream, multilayer radiative approximation of [*Toon et al*., 1989]. The optical properties for snow particles (grain sizes between 10 μm and 5 mm at 1 μm resolution), BC, and dust in four size bins (0.01–1.0 μm, 1.0–2.5 μm, 2.5–5.0 μm, and 5.0–10 μm) are extracted from lookup tables. In addition to impurity concentration,

user specified inputs include solar zenith angle and snow properties, number and depth of snow layers, and density and optical grain size within each layer.

In our runs, we treat the snowpack as two layers, with a 3 cm surface layer where impurities are specified, below which lies a 5 m snowpack containing the average impurity concentration sampled across the shallow ice core not including the 2011 summer surface layer (section 3.2). Dust size bin partitioning was based on the particle size distribution from the 2011 summer surface impurity layer, measured with laser light diffraction (Mastersizer 2000). Particle sizes ranged from ~5 to 35 μm, with 3% of volume fraction in size bin 1, 13% in size bin 2, 18% in size bin 3, and 66% in bin 4 (dust particles larger than 10.0 um were included in bin 4). This was the only sample for which a particle size distribution was measured because particle concentrations in other samples were too low to allow a measurement to be made. Thus, we apply the measured particle size to distribution to all model runs under the assumption that summer 2012 dust would be similar. While this assumption introduces uncertainty into modeled albedo, we assessed the sensitivity of the size bin distribution in test runs by shifting the lognormal distribution such that the volume mean peak radius was either 50% larger or smaller and found that the change in albedo was $<1\%$ for the dust concentrations sampled in 2012.

We use a measured optical grain size, and density inferred from the mass and volume of surface samples, both collected during the August 2012 field campaign. Optical grain size, which is the radius of the equivalent sphere that returns the same hemispherical flux, is inferred from the ice absorption feature centered at 1.03 microns, retrieved from the contact spectroscopy spectral flux measurements with the field spectrometer [*Painter et al*., 2007].

The output from SNICAR is spectral albedo between 0.3 and 5.0 μm at 0.010 μm resolution. Spectrally weighted albedo is estimated by applying this to midlatitude summer solar irradiance modeled from SBDART (Santa Barbara discrete ordinates radiative transfer atmospheric radiative transfer model) [*Ricchiazzi et al*., 1998] at the elevation of Snow Dome, between 0.35 and 2.5 μm at the same 0.010 μm spectral resolution:

$$\alpha = \frac{\sum_{\lambda=0.35\,\mu m}^{2.5\,\mu m} I_\lambda * \alpha_{\lambda_{LAI}} \Delta\lambda}{\sum_{\lambda=0.35\,\mu m}^{2.5\,\mu m} I_\lambda \Delta\lambda}$$

where I_λ is the modeled spectral irradiance at specified solar zenith angle, $\alpha_{\lambda lai}$ is the modeled spectral albedo with BC/dust at the same solar zenith angle, and λ is the wavelength (μm).

Radiative forcing, in W m^{-2}, is the difference in albedo modulated reflected flux between the clean and LAI laden runs:

$$RF = \sum_{\lambda=0.35\,\mu m}^{2.5\,\mu m} I_\lambda * (\Delta\alpha_\lambda)\Delta\lambda$$

where $\Delta\alpha_\lambda = \alpha_{clean} - \alpha_{lai}$, which is the difference between clean snow albedo and dust/BC albedo.

Both SBDART and SNICAR model runs were produced for clear and cloudy sky conditions at an hourly time step. Cloudy conditions were represented in SBDART with a fractional cloud cover of 1 and an optical depth of 10 at 0.55 μm. Solar zenith angles were calculated for the latitude/longitude of Snow Dome between 6:00 A.M. and 6:00 P.M. to represent solar irradiance and snow albedo over a full day. These solar zenith angles capture the majority of daylight hours during late summer. During late August (timing of measurements in 2012) and early September (timing of fire deposition in 2011), the sunrise occurs between 5:00 A.M. and 6:00 A.M. (PDT), solar noon is just after 12:00 P.M., and Sun sets between 6:30 P.M. and 7:30 P.M. At each hour, we calculated the equal weight average of the clear and cloudy forcings, and then integrated over the day to produce all-sky 12 h daily mean radiative forcings.

3. Results and Discussion

3.1. BC and Dust Concentrations in Surface Snow and Measured Spectral Albedo

We use the gravimetric data and the iron (Fe) ICP-SFMS data to infer spatial variations in dust concentrations. Fe was selected as the ICP-SFMS dust proxy because iron oxides dominate light absorption by mineral dust

Table 1. Measured Black Carbon (BC), Iron (Fe), and Gravimetric Dust in Surface Snow Samples From the 2012 Summer (Sites 1–4) and the 2011 Summer Horizon in the Snow Dome Ice Core (Site 1—2012), and Measured Broadband Albedo for Surface Snow in Summer 2012

Site	BC (ug/L)	Fe (ug/L)	Gravimetric Dust (mg/L)	BC/Gravimetric Dust × 10^{-3}	Broadband Albedo
1	19	299	-	-	0.74
1	18	-	-	-	0.74
1	21	425	27	0.8	0.74
2	120	-	-	-	0.67
2	140	-	-	-	0.67
2	72	728	62	1.2	0.67
3	24	299	30	0.8	0.70
4	17	84	24	0.7	0.73
1-2012	3120	22000	1870	1.7	-

[*Lafon et al.*, 2004]. BC (min = 17 μg/L, max = 140 μg/L, average = 54 μg/L, $n = 9$) and dust proxy concentrations (Fe min = 84 μg/L, max = 728 μg/L, average = 367 μg/L, $n = 5$; gravimetric min = 24 mg/L, max = 62 mg/L, average = 36 mg/L, $n = 4$) in surface snow collected on Snow Dome (Figure 1c) were spatially variable. This is consistent with the spectral albedo measured at seven sites on Snow Dome, with higher concentrations of BC and dust corresponding to lower measured spectral albedo (Table 1 and Figures 1–3). Previous researchers have documented high spatial variability of impurity concentrations in surface snow at this site associated with the formation of ablation hollows [*Rhodes et al.*, 1987].

3.2. BC and Fe Concentrations in the Shallow Ice Core

The BC and Fe concentrations measured in the shallow ice core were lower (BC ≤ 1 μg/L; Fe ≤ 6 μg/L) than those measured in the 2012 surface snow, with the exception of a very high concentration impurity layer at 6.8 m depth (BC = 3120 μg/L, Fe = 22000 μg/L, and gravimetric = 1870 mg/L) (Figure 4 and Table 1).

We interpret the high impurity layer at 6.8 m depth as marking the 2011 summer horizon, consistent with previous research that documented the highest LAI impurity concentrations on glaciers in Washington State occur during summer [*Delaney*, 2013]. During the winter, snowfall is high, which results in impurities being diluted in the snowpack, whereas during the relatively dry summer the impurities are concentrated at the snow surface.

To verify that the 2011 summer layer was located at 6.8 m depth, we determined that 6.8 m of snow accumulated during the 2011 and 2012 winter would remain on Snow Dome in September 2012. We used the approach of *Rasmussen et al.* [2000], in which temperature and precipitation data are used to estimate snowfall on Blue Glacier. Based on this approach, snowfall equivalent to 3.7 m water equivalent is accumulated on Blue Glacier during the 2011 to 2012 winter. This is equivalent to 7.4 m snow depth assuming snow density of 0.5 kg/m^3, consistent with density observations from this time of year [*Conway et al.*, 1996]. While some of the accumulated snow would have ablated during summer, the summer of 2012 had notably above average retained snowpack above 1500 m in this region (M. Pelto, personal communication, 2014). When accounting for spatial variability in snow accumulation on Snow Dome and errors inherent to the *Rasmussen et al.* approach, that the 2011 summer horizon is located at 6.8 m depth in the ice core is reasonable.

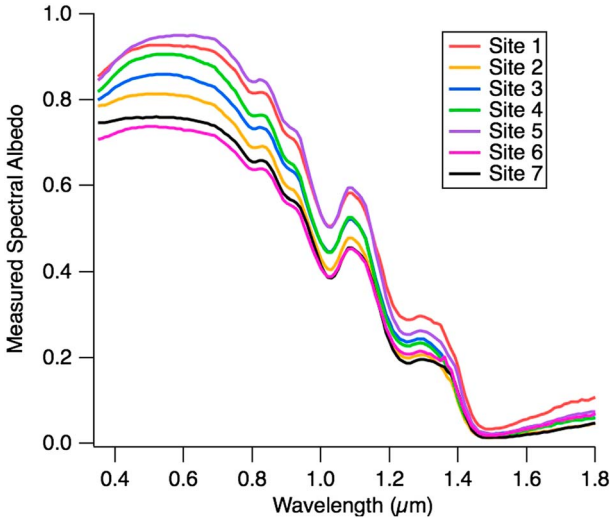

Figure 2. Measured spectral albedo on Snow Dome during August 2012. Site numbers correspond to geochemical data presented in Table 1.

We exclude the possibility that the high impurity layer recorded in the ice core at 6.8 m depth represents more than 1 year of impurity deposition that coalesced into a single layer. Snowfall during the winters of 2010–2011 and

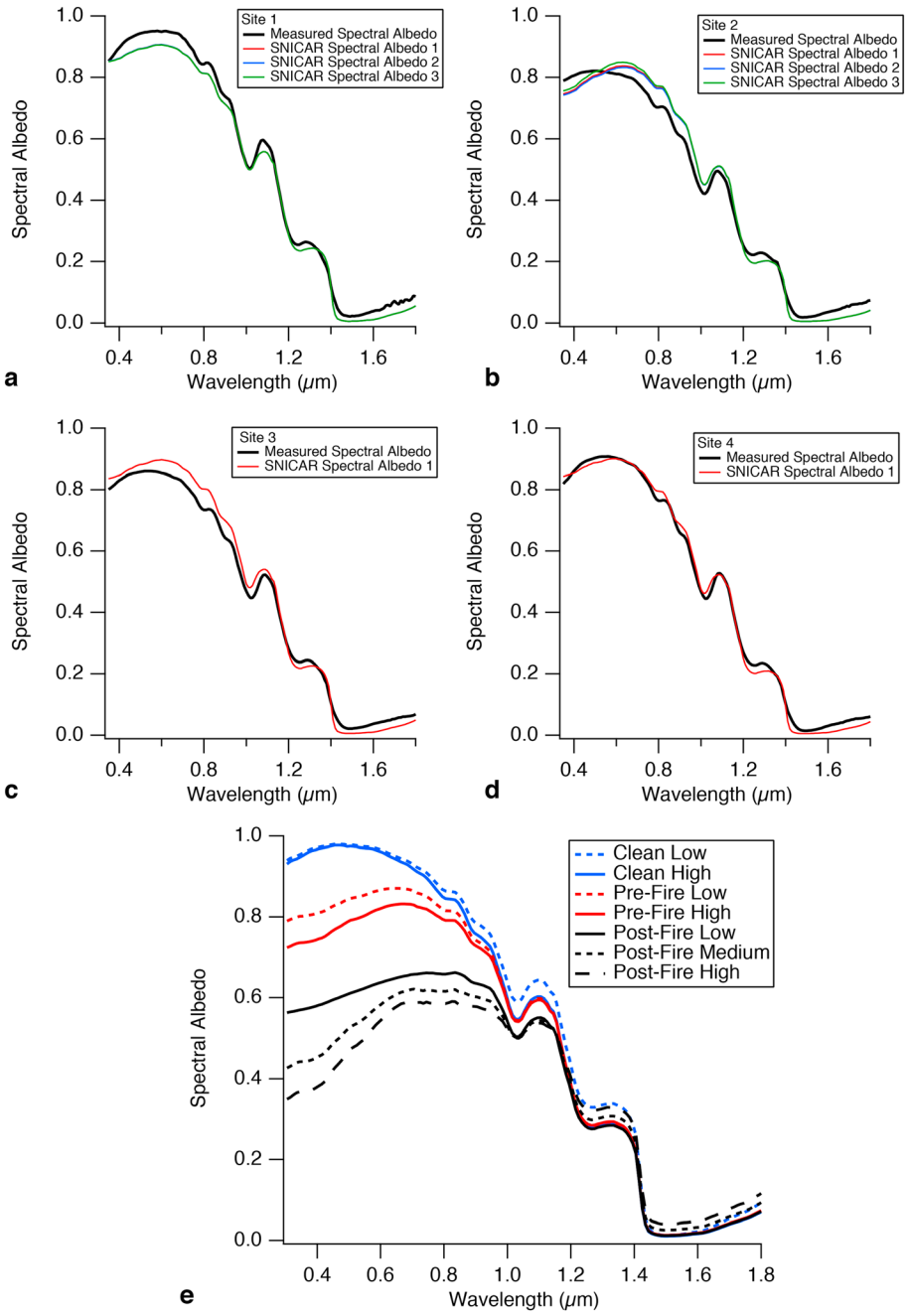

Figure 3. Measured and SNICAR modeled snow spectral albedo from Snow Dome during August 2012 for sites (a) 1, (b) 2, (c) 3, and (d) 4 based on observed black carbon, gravimetric dust, optical grain radii, and clear-sky conditions (see values reported in Table 1). For sites 1 and 2, three SNICAR results are presented corresponding to the gravimetric dust concentration and the three black carbon concentrations measured at these two sites. For site 1, the difference in the three SNICAR runs is not distinguishable due to little variation in the measured black carbon concentrations. (e) SNICAR modeled spectral albedo based on the clean snow, prefire, and postfire scenarios reported in Table 2 based on clear-sky conditions.

2011–2012 was the highest and third highest recorded, respectively, based on the Waterhole Snowpack Telemetry site (47.95°N, 123.44°W, 1527 m; record spans 2000–2014) (Figure 1). Additionally, the 2011 and 2012 end of summer snowline on Blue Glacier was located at 1550 m and 1700 m, respectively, based on end of summer aerial photographs. This level is well below the elevation where the shallow ice core was drilled (2080 m), indicating that the end of summer mass balance on Snow Dome was positive in both 2011 and 2012.

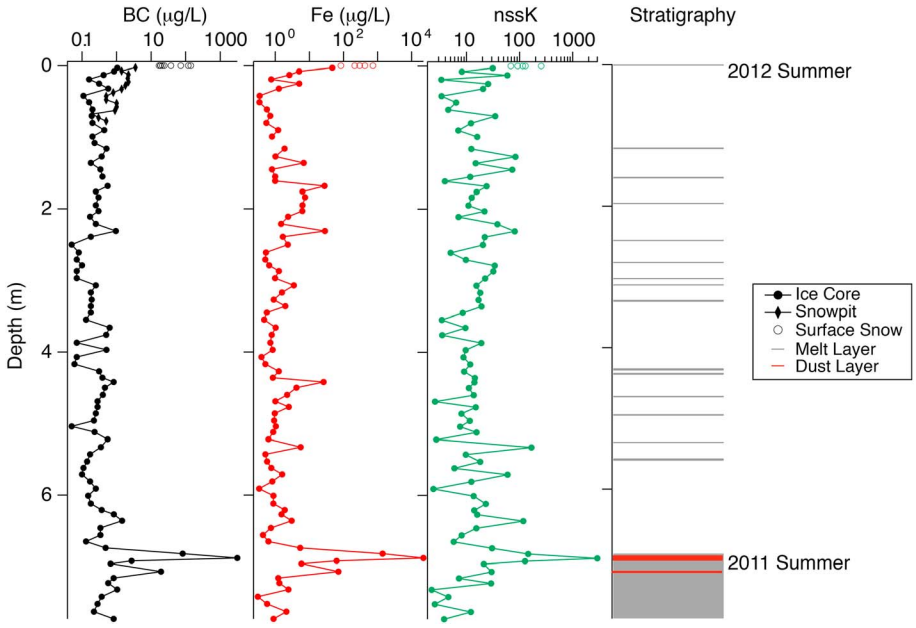

Figure 4. Black carbon (BC), iron (Fe), non-sea salt potassium (nssK), and visual stratigraphy data from the Snow Dome shallow ice core.

3.3. Large Impurity Layer Caused by the 2011 Big Hump Fire

The BC and dust concentrations in the 2011 summer horizon are considerably higher than the maximum measured in the surface snow during August 2012, and in 2011 the contribution of BC to the total impurity load was also higher (Table 1). Our field sampling on Snow Dome took place the week of 20 August 2012. Thus, in 2012, BC and dust deposition during the rest of August and September was not captured. While this could in part explain why measured BC and dust deposition in 2012 was considerably lower than in 2011, we suggest other factors must have contributed to the high 2011 BC and dust concentrations.

Another possibility is that BC deposited during 2012 was flushed through the snowpack and consolidated at the 2011 horizon. Previous studies have documented that BC can migrate through the snowpack during conditions of melt [*Conway et al.*, 1996; *Xu et al.*, 2012]. While relatively thin (<1 cm) melt layers were observed in the upper 6.8 m of the ice core, visual inspection did not indicate the occurrence of strong melt that would have enabled BC and dust to be flushed over 6 m through the snowpack. Furthermore, the BC concentration measured in the 2011 summer horizon was markedly higher than concentrations typically observed in this region [*Delaney*, 2013], and coalescence of 2 years of impurities would not explain the high concentrations observed in the 2011 summer horizon. In investigating other sources of BC that could have contributed to the high 2011 summer horizon, we determined that the 2011 Big Hump fire on the Olympic Peninsula was very likely the source of the elevated BC.

The 2011 Big Hump fire (47.70°N, 123.10°W) was ignited on 31 August 2011 near the Duckabush River 47 km southeast of Snow Dome. The fire spread quickly into steep, rugged terrain with heavy fuel, resulting in 5.6 km^2 of forest burned during September 2011. Big Hump is located predominantly downwind of Mount Olympus, but atmospheric balloon sounding data from Quillayute (47.95°N, 124.55°W) (Figure 1) on the Olympic Peninsula indicates periods of southeasterly winds between 800 and 900 mb on 3, 7, 8 and 10 September that allowed emissions from the Big Hump fire to be transported to Snow Dome (Figure 5). Atmospheric elemental carbon (EC, comparable to BC but is instead thermally defined) at the Makah site from the IMPROVE (Interagency Monitoring of Protected Visual Environments) network, which provides a 24 h measurement of EC every third day, was also elevated on 3 and 9 September, with measured EC on 9 September the highest measured concentration in 2011 during the nonwinter months. Southeasterly winds would enable the transport of BC from the Big Hump fire to Mount Olympus and Makah (Figures 1 and 5). Additionally, hazy air quality typical of forest fire emissions was observed over Mount Olympus and the surrounding area during 7–9 September 2011 (Figure 6) (B. Baccus, personal communication, 2013).

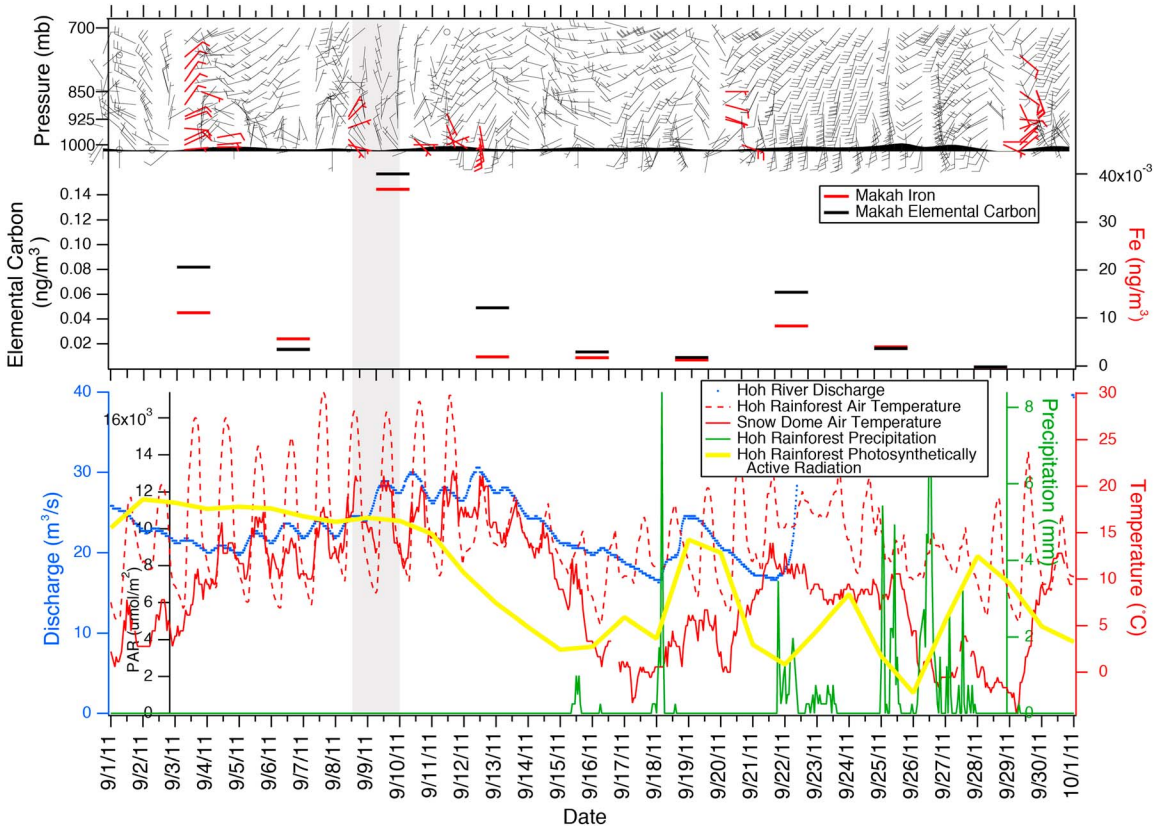

Figure 5. Instrumental data from the Olympic Peninsula during September 2011, corresponding to the timing of the Big Hump fire. (a) Wind barb data versus pressure from Quillayute (easterly and southeasterly winds are in red bold), (b) atmospheric elemental carbon (ng/m^3) and Fe (ng/m^3) concentrations from the Makah IMPROVE site, and (c) Hoh river discharge (m^3/s), Hoh rainforest and Snow Dome air temperature (°C), Hoh rainforest precipitation (mm), and Hoh rainforest photosynthetically active radiation (μmol/m^2). The vertical gray bar highlights the most likely period of time when LAI from the Big Hump fire was deposited on Snow Dome.

Geochemical analysis of the ice core supports that the elevated BC concentrations in 2011 originated from forest fire. Microscopic charcoal analysis identified the presence of charcoal in the 2011 summer horizon. Additionally, non-sea salt potassium (nssK) calculated according to [*Keene et al.*, 1986] that is commonly used as a tracer of biomass burning [*Engling et al.*, 2011] was also elevated in the 2011 summer horizon (Figure 4). While the forest fire likely contributed to the elevated nssK, some of the nssK likely has a dust source (discussed below).

Measurements with the integrating sphere/spectrometer of impurities spectral albedo for the 2011 summer horizon relative to the 2012 summer horizon also suggest that the 2011 impurity mixture has a higher volume fraction of a dark absorber like BC (Figure 7). Across the solar wavelengths, dust absorption varies spectrally, while the magnitude of absorption depends upon the mineral composition. In general, dust is

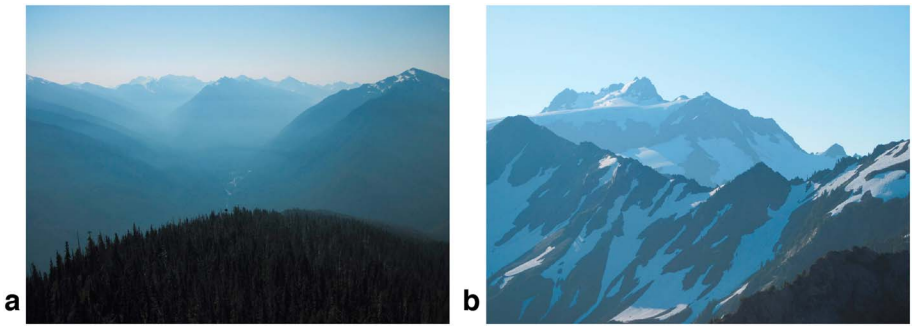

Figure 6. Pictures taken of haze over (a) the upper Elwha Valley and (b) Mount Olympus on 8 September 2011, a period of southeasterly winds during the Big Hump fire. Photos by Bill Baccus.

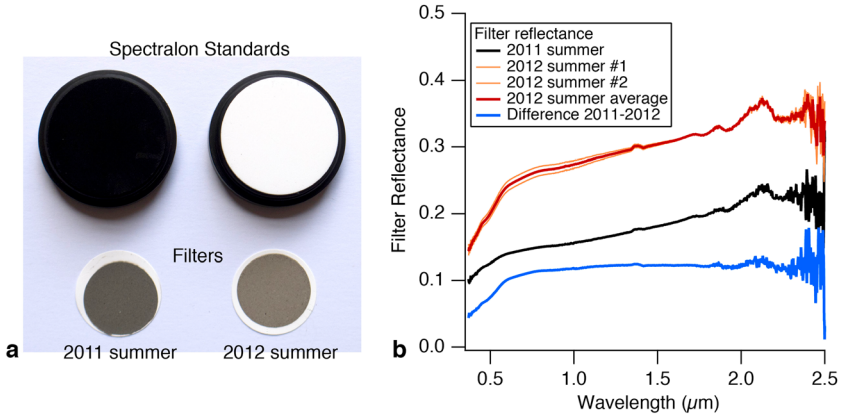

Figure 7. (a) Picture of impurities captured on Millipore filters from snow/ice from the 2011 and 2012 summers from Snow Dome, and black and white spectralon standards for comparison. (b) Filter reflectance measured with the spectrometer for 2011 and 2012 summer, and reflectance difference between the 2 years. For 2012, filter reflectance was measured for sites 3 (summer #1) and 4 (summer #2). There was minimal spectral variation between the two filters, and the difference was taken from the average reflectance of the two filters.

most absorbing around 0.3 μm, becomes less absorbing across the visible wavelengths, and then levels out between ~0.75 μm and 2.5 μm [*Sokolik and Toon*, 1999]. Absorption by BC is fairly constant between 0.35 and 2.5 μm and is not considered to be wavelength dependent [*Bond and Bergstrom*, 2006]. Therefore, the more BC that is contained within an impurity would result in less spectral variation across the visible wavelengths and a decrease in overall reflectance, as exhibited in Figure 7.

We conclude that the Big Hump fire is the dominant source of impurities in the 2011 summer horizon. Furthermore, the fire impurity radiative forcing may have accelerated melt and in turn reinforced the concentration of impurities. However, because the BC and dust from summer 2011 are concentrated in a single horizon, it is not clear how much of the dust was deposited before, during, or after the Big Hump fire. Previous studies have reported elevated atmospheric Fe concentrations due to forest fire emissions [*Guieu et al.*, 2005], thus some of the Fe may have originated from Big Hump fire emissions. However, the Fe/Al ratio is not elevated in the 2011 summer horizon, indicating that dust is likely the dominant source of the higher Fe concentrations. At least some of the dust may be related to the fire, as dust emissions are known to markedly increase in burned areas relative to nonburned areas [*Whicker et al.*, 2006]. This is supported by elevated dust concentrations recorded at the Makah IMPROVE site on 9 September 2011 (Figure 5), with positive matrix factorization modeling of the Makah IMPROVE data indicating that, on this date, aerosol emissions are dominated by dust and combustion (O. Hadley, personal communication, 2014). As discussed earlier, this corresponds to the time when southeasterly winds provided a mechanism by which emissions from Big Hump could be transported to Olympus and Makah.

3.4. Snow Albedo Reductions and Estimated Radiative Forcing due to Deposition of BC and Dust

The deposition of BC and dust on Snow Dome lowers the surface albedo, causes a positive radiative forcing, and increases melt. Here we investigate the impact of impurity deposition from the Big Hump fire on melt using measured snow properties and radiative transfer modeling.

We assess SNICAR's ability to represent observed conditions by comparing SNICAR spectral albedo results to spectral albedo measured during the August 2012 field campaign (Figures 2 and 3). These model runs are forced with the solar zenith angle, measured optical grain size, snow density, and impurity concentrations that correspond to the time and location albedo was measured. The SNICAR modeled albedo agreed well with the measured albedo, with the difference between measured and modeled broadband albedo (0.35–1.8 μm) ranging from +0.03 to −0.03, with an average underestimation of <0.001 or 0.3% difference. At site 4, modeled broadband albedo was only 0.002 lower than measured albedo, whereas the largest difference was at site 1, where modeled broadband albedo was 0.03 lower than measured albedo. Differences between measured and modeled albedo were largest across the visible wavelengths (0.35–0.75 μm) and ranged from 0.04 to −0.03.

Differences between measured and modeled albedo can be put in terms of a reflected solar flux error by applying spectral albedo to spectral irradiance modeled with SBDART that corresponds to the time of albedo

Table 2. Inputs Used for the SNICAR Modeling Scenarios Described in the Text and Presented in Figures 3 and 8, and Modeled Broadband Albedo

Scenario	BC (ug/L)	Gravimetric Dust (mg/L)	Optical Grain Radius (um)	Broadband Albedo (Clear Sky)	Broadband Albedo (Cloudy Sky)
Clean low	-	-	393	0.77	0.84
Clean high	-	-	520	0.75	0.82
Prefire low	140	62	520	0.68	0.73
Prefire high	280	124	520	0.65	0.70
Postfire low	3120	62	520	0.52	0.56
Postfire medium	3120	900	520	0.48	0.53
Postfire high	3120	1870	520	0.45	0.49

collection. The broadband flux errors ranged from +26 (site 1) to $-22\,W\,m^{-2}$ (site 4) and were $-0.5\,W\,m^{-2}$ on average. The visible flux errors ranged from +20 to −15 and were $+2\,W\,m^{-2}$ on average. The near-infrared flux errors ranged from +6 to −7 and were $-2\,W\,m^{-2}$ on average. The lower near-infrared errors are attributed to using a measured grain size, whereas the higher variability across the visible is attributed to uncertainty in measured impurity concentrations and/or the optical properties used in SNICAR not coming from this region. Additionally, SNICAR uses a single mass absorption coefficient for BC, but this likely varies with particle size [*Schwarz et al.*, 2013]. Given these results, a reasonable maximum uncertainty for the following radiative forcing results, due to albedo modeling, is $\pm 20\,W\,m^{-2}$.

To estimate radiative forcing due to deposition of impurities from the Big Hump fire, we used sampled snow properties in 2012 and the 2011 summer horizon BC and dust concentrations. For preforest fire event impurity loading, we use two scenarios, which are based on the surface concentrations and snow properties measured at site 2 (coring site) in August 2012. The first preforest fire scenario is the low impurity scenario that assumes the 2012 impurity loading is representative of summer impurity loading at Snow Dome and is constrained by measurements of concentrations, optical grain size, and snow density (140 μg/L BC, 62 mg/L dust, 520 μm optical grain size, and 500 kg/m^3 density). The second preforest fire scenario is the high impurity scenario, in which the measured August 2012 BC/dust concentrations are doubled to account for additional impurity deposition that may have occurred in late August and September but not have been captured during the 2012 field campaign (22–24 August 2012) (Table 2).

Based on our understanding of the 2012 horizon, the 2011 fire likely deposited the majority of BC sampled at the 2011 horizon, but as previously discussed, the timing of dust deposition cannot be similarly constrained; therefore, three postfire radiative forcing scenarios were used for various dust loadings. The minimum estimate uses the same amount of dust measured in 2012 (62 mg/L), the maximum estimate uses the amount of dust measured at the 2011 horizon (1870 mg/L), and the middle estimate uses roughly the average between the two (900 mg/L). Measured BC is held constant across these scenarios, such that variation in postfire radiative forcing is due only to changes in dust concentration. Postfire scenarios use the same measured grain size and snow density as prefire runs, so that radiative forcing comparisons are constrained to absorption by impurities. Given that grain size is enhanced by the presence of impurities, the optical grain radii measured in 2012 were likely smaller than surface grain sizes postfire in 2011, which would make this a conservative estimate of 2011 surface albedo, but this is unknowable. Using measurements at the ice core site alone does not capture spatial variability in impurity deposition that likely existed on Snow Dome in 2011 but nonetheless provides a valuable measurement of impurity deposition from 2011.

Estimates of radiative forcing, the enhanced surface absorption that can be attributed to impurities, require estimates of clean snow albedo. In the absence of impurities, inherent snow albedo is inversely related to snow grain size; and for clean snow scenarios, we model snow albedo using both the smallest (393 μm) and largest (520 μm) measured optical grain radii in 2012. Since postfire and prefire scenarios also utilize 520 μm, the difference between these scenarios represents direct absorption by impurities across the visible wavelengths. The difference in absorption between the impurity scenarios and 393 μm clean snow scenario gives an estimate of both the direct (snowmelt and concentration of impurities are driven by energy absorption of the impurities in snow) and indirect (accelerated grain growth from the direct effect results in larger snow grain size and lower near-infrared reflectance) effects of impurities. We have restricted this analysis to

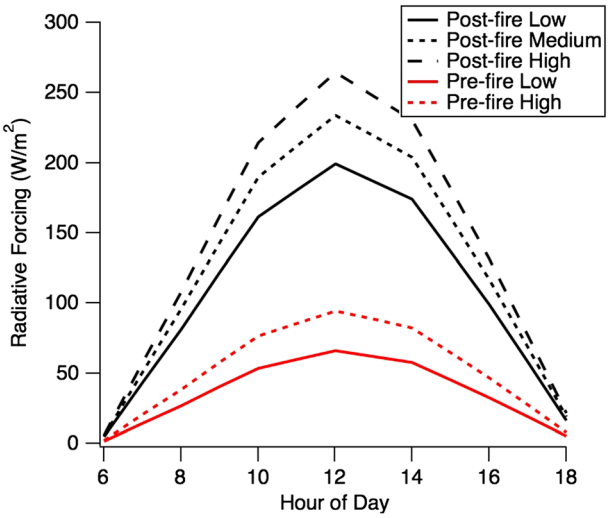

Figure 8. Hourly all-sky radiative forcing (W m^{-2}) for the scenarios presented in Table 2.

measured grain radii, which cannot be decoupled from enhanced grain growth due to the dust/BC that was present in 2012; and, therefore this is likely a conservative estimate of both clean snow reflectance and radiative forcing. For reported radiative forcing, we use the average of the two clean snow scenarios.

Daily mean all-sky radiative forcings by preforest fire BC/dust concentrations were estimated to be 37 W m^{-2} (low scenario) to 53 W m^{-2} (high scenario), with instantaneous forcings at solar noon of 65 W m^{-2} and 94 W m^{-2} (Figure 8). Daily mean radiative forcings by postfire scenarios were 112 W m^{-2} (low scenario), 132 W m^{-2} (medium scenario), and 148 W m^{-2} (high scenario) with instantaneous forcings of 199 W m^{-2} (low scenario), 234 W m^{-2} (medium scenario), and 264 W m^{-2} (high scenario) at solar noon (Figure 8). Depending on the scenario, the postfire forcings were 2–4 times higher than the prefire forcings. The majority of the postfire radiative forcing is attributed to the higher BC content deposited by the fire, as increasing dust from 62 mg L^{-1} to 900 mg L^{-1} increases daily radiative forcings by 20 W m^{-2}, 15% of the medium scenario radiative forcing, and further doubling that concentration adds an additional 16 W m^{-2}, 10% of the high scenario radiative forcing.

3.5. Impact of BC and Dust Deposition on Melt and Runoff

Using the additional energy contribution to the snowpack due to BC and dust deposition described in section 3.4, we can make a first-order estimate of the impact on snowmelt by doing a simple energy analysis. We must make the assumption that the snow is at the melting point, such that the additional energy is not contributing to raising the temperature of the snow to 0°C. This assumption is reasonable, as late summer observed near-surface snow temperatures on Blue Glacier range between −0.02 and +0.001°C [*Harrison*, 1975]. In this scenario, we estimate the additional melt from LAI by dividing hourly instantaneous radiative forcing by the enthalpy of fusion of water at 0°C (0.334×10^6 J kg^{-1}), to return melt in kg m^{-2}, equivalent to millimeter of snow water equivalent. This approach is also found in *Painter et al.* [2013b] for an annual snowpack with a known total snow water equivalent (SWE) to estimate the rate at which LAI radiative forcing would deplete the total snow cover. At Snow Dome the snow cover is permanent, so here we simply want to estimate the degree of increased runoff postfire. Prefire radiative forcing results in an average daily enhanced SWE reduction of 9 mm (prefire low scenario) to 13 mm (prefire high scenario). Postfire radiative forcing results in an average daily SWE reduction of 29 mm (postfire low scenario) to 38 mm (postfire high scenario). Following the magnitude of radiative forcing increase, postfire impurity loading increases prefire SWE reduction by a factor of 2–4.

To see if the postfire increase in SWE reduction was detectable, we examined discharge data from the Hoh River, the catchment river for Snow Dome (discharge data from the United States Geological Survey; Figures 1 and 5), and local climate data (including air temperature, precipitation, and photosynthetically active radiation data >from the Hoh Rainforest site, Olympic National Park, and Snow Dome temperature data from SuomiNet) [*Ware et al.*, 2000] (Figures 1 and 5). During the first 2 weeks of September there was no precipitation, so factors other than precipitation cause the observed discharge variations during this time. From 9–13 September 2011 there was a marked increase in Hoh River discharge. The largest daily change in runoff occurred on 9 September, with a daily average increase of 3.7 m^3/s, which is more than triple that of the next largest change in discharge during this 2 week period. Slight temperature increases that began on 7 September at the Hoh Rainforest site and 8 September at Snow Dome were sustained during the period of greater discharge from 9 to 13 September, suggesting that temperature contributed to the discharge

increase. However, the increase in discharge that occurred on 7 and 8 September when temperature first increased is moderate. Thus, the higher discharge observed on 9 September and sustained through 13 September resulted either from a delay in temperature driven snowmelt entering the Hoh River or other factors driving the discharge increase. The timing of discharge increase on 9 September corresponds to the estimated timing of BC deposition from the Big Hump fire (Figure 2), which suggests that the BC deposition event may have contributed to the observed increase in discharge at this time.

However, this analysis is speculative because in addition to the amount of snow available to melt and snow energy balance, there are a number of factors that influence runoff and discharge including basin hypsometry and snowpack/soil column lags. If we had energy balance measurements (i.e., net shortwave and longwave energy flux, air temperature, wind speed, relative humidity, and precipitation), we could have modeled snowpack accumulation and melt at Snow Dome to assess the impact of impurities on snowpack outflow following an approach similar to that found in *Skiles et al*. [2012]. Without more knowledge of the hydrology dynamics within the basin, or discharge measurements closer to the pour point of the subbasin containing Snow Dome, it would be difficult to directly correlate the discharge increase to the sampled impurities. Additionally, a small precipitation event on 15 September and a larger one on 22 September prevent us from investigating the impact on runoff over a long time period.

4. Conclusions

We documented BC and dust deposition on Snow Dome, Mount Olympus that was a magnitude higher in 2011 than 2012, and identified the 2011 Big Hump forest fire on the Olympic Peninsula as the source of the greatly elevated impurity deposition. The forest fire impurity deposition reduced albedo, increased the radiative forcing, and enhanced snowmelt. The timing of impurity deposition from the Big Hump fire was coincident with an increase in observed discharge in the Hoh River that is not related to changes in precipitation or radiation. Our analysis suggests that while an increase in temperature may have contributed to the rise in discharge, enhanced melt by deposited impurities also may have contributed to the discharge increase.

This study highlights the potential for BC and dust emissions from forest fires to be deposited on glaciers and accelerate melt. While prior studies have largely focused on the linkage between forest fire and snow and glacier melt due to changes in the forest canopy [*Burles and Boon*, 2011; *Harpold et al*., 2014], few studies have documented the deposition of forest fire emissions on snow and glaciers. *Keegan et al*. [2014] documented that widespread melt on the Greenland ice sheet in 2012 was caused by higher temperatures and BC from forest fires that occurred in North America and Siberia, and *Kim et al*. [2005] suggested that northern boreal forest fires may accelerate glacier melt in Alaska and sea ice melt in the Arctic from BC deposition. The results presented here provide the first linkage of BC deposition from an identified forest fire to enhanced discharge, though more data are needed to solidify this relationship. Additionally, this is the first study to highlight forest fire impacts on glacier melt in the midlatitudes.

In Washington State, high-elevation snowpacks and glacier melt can buffer streamflow during the relatively dry summer, thus the potential for forest fires to affect melt is of interest. This region has a long fire history [e.g., *Wendel and Zabowskl*, 2009], both from lightning and human ignited fires. On the Olympic Peninsula, particularly on the drier eastern side of the peninsula, forest fires occur regularly. Changes in forest management have contributed to an increase in acreage burned in recent years, including the 2003 Griff fire (3.3 km^2), the 2009 Heatwave Complex (6.1 km^2), the 2010 Hopper fire (1.5 km^2), and the 2011 Big Hump fire (5.6 km^2) (National Park Service). Understanding the linkage between forest fire and melt is of interest, particularly in the context of a changing climate where the area burned by forest fire and fire intensity will increase and continued glacier retreat is projected [*Littell et al*., 2009; *Yue et al*., 2013].

Acknowledgments

This research was supported by the United States Geological Survey/State of Washington Water Research Center (2012WA344B) and the Office of the Dean, College of the Sciences, Central Washington University, Ellensburg, Washington. S.M. Skiles and T.H. Painter were covered under NASA project NNX10A097G. Part of this work was performed at the Jet Propulsion Laboratory, California Institute of Technology under a contract with NASA. We thank Bill Baccus at Olympic National Park for help planning field logistics and providing local climate data; Mike Tetreau for assistance in the field; Megan Weyand for ice core processing; Megan Walsch for charcoal analysis; Paul Mayewski and Mike Handley for ICP-SFMS data analysis; Levi Windingstad for conducting the particle size distribution measurement; Joel Barker for epifluorescence analysis; Larry Oolman for access to sounding data; Bryon Free for assistance with mapping; and Twit Conway, Al Rasmussen, and Jon Riedel for valuable conversations about snow accumulation on Washington glaciers. Rasmussen conducted the 2011 and 2012 snowfall calculations presented in section 3.2. The full data set from this study is available by emailing kaspari@geology.cwu.edu.

References

Bond, T., and R. Bergstrom (2006), Light absorption by carbonaceous particles: An investigative review, *Aerosol Sci. Technol.*, *40*, 27–67.

Bond, T. C., D. G. Streets, K. F. Yarber, S. M. Nelson, J. H. Woo, and Z. Klimont (2004), A technology-based global inventory of black and organic carbon emissions from combustion, *J. Geophys. Res.*, *109*, D14203, doi:10.1029/2003JD003697.

Bond, T., E. Bhardwaj, R. Dong, R. Jogani, S. Jung, C. Roden, D. G. Streets, and N. Trautmann (2007), Historical emissions of black and organic carbon aerosol from energy-related combustion, 1850–2000, *Global Biogeochem. Cycles*, *21*, GB2018, doi:10.1029/2006GB002840.

Burles, K., and S. Boon (2011), Snowmelt energy balance in a burned forest plot, Crowsnest Pass, Alberta, Canada, *Hydrol. Processes*, *25*(19), 3012–3029, doi:10.1002/hyp.8067.

Clarke, A. D., and K. J. Noone (1985), Soot in the Arctic snowpack: A cause for perturbations in radiative transfer, *Atmos. Environ.*, *19*(12), 2045–2053.

Conway, H., A. Gades, and C. F. Raymond (1996), Albedo of dirty snow during conditions of melt, *Water Resour. Res.*, *32*, 1713–1718, doi:10.1029/96WR00712.

Conway, H., L. A. Rasmussen, and H. P. Marshall (1999), Annual mass balance of Blue Glacier, USA: 1955–97, *Geogr. Ann. Ser. A-Phys. Geogr.*, *81A*(4), 509–520.

Delaney, I. (2013), *Black Carbon Deposition on Snow and Glaciers in Washington State: Implications for Accelerated Snowmelt*, MS thesis, 169 pp., Central Washington Univ., Ellensburg.

Eichler, A., W. Tinner, S. Brutsch, S. Olivier, T. Papina, and M. Schwikowski (2011), An ice-core based history of Siberian forest fires since AD 1250, *Quat. Sci. Rev.*, *30*(9–10), 1027–1034.

Engling, G., Y.-N. Zhang, C.-Y. Chan, X.-F. Sang, M. Lin, K.-F. Ho, Y.-S. Li, C.-Y. Lin, and J. J. Lee (2011), Characterization and sources of aerosol particles over the southeastern Tibetan Plateau during the Southeast Asia biomass-burning season, *Tellus, Ser. B*, *63*(1), 117–128, doi:10.1111/j.1600-0889.2010.00512.x.

Flanner, M. G., and C. Zender (2005), Snowpack radiative heating: Influence on the Tibetan Plateau climate, *Geophys. Res. Lett.*, *32*, L06501, doi:10.1029/2004GL022076.

Flanner, M. G., and C. Zender (2006), Linking snowpack microphysics and albedo evolution, *J. Geophys. Res.*, *111*, D12208, doi:10.1029/2005JD006834.

Gleason, K. E., A. W. Nolin, and T. R. Roth (2013), Charred forests increase snowmelt: Effects of burned woody debris and incoming solar radiation on snow ablation, *Geophys. Res. Lett.*, *40*, 4654–4661, doi:10.1002/grl.50896.

Grenfell, T. C., D. K. Perovich, and J. A. Ogren (1981), Spectral albedos of an alpine snowpack, *Cold Reg. Sci. Technol.*, *4*, 121–127.

Guieu, C., S. Bonnet, T. Wagener, and M.-D. Loÿe-Pilot (2005), Biomass burning as a source of dissolved iron to the open ocean?, *Geophys. Res. Lett.*, *32*, L19608, doi:10.1029/2005GL022962.

Harpold, A. A., J. A. Biederman, K. Condon, M. Merino, Y. Korgaonkar, T. Nan, L. L. Sloat, M. Ross, and P. D. Brooks (2014), Changes in snow accumulation and ablation following the Las Conchas Forest Fire, New Mexico, USA, *Ecohydrology*, *7*(2), 440–452.

Harrison, W. D. (1975), Temperature of a temperate glacier, *J. Glaciol.*, *14*(70), 23–30.

Joseph, J. H., W. J. Wiscombe, and J. A. Weinman (1976), The delta-Eddington approximation for radiative flux transfer, *J. Atmos. Sci.*, *33*(12), 2452−2459.

Kaspari, S., T. H. Painter, M. Gysel, S. M. Skiles, and M. Schwikowski (2014), Seasonal and elevational variations of black carbon and dust in snow and ice in the Solu-Khumbu, Nepal and estimated radiative forcings, *Atmos. Chem. Phys.*, *14*, 1–15.

Keegan, K. M., M. R. Albert, J. R. McConnell, and I. Baker (2014), Climate change and forest fires synergistically drive widespread melt events of the Greenland ice sheet, *Proc. Natl. Acad. Sci. U.S.A.*, *111*(22), 7964–7967, doi:10.1073/pnas.1405397111.

Keene, W. C., A. A. P. Pszenny, J. N. Galloway, and M. E. Hawley (1986), Sea-salt corrections and interpretation of constituent ratios in marine precipitation, *J. Geophys. Res.*, *91*(D6), 6647−6658, doi:10.1029/JD091iD06p06647.

Kim, Y., H. Hatsushika, R. R. Muskett, and K. Yamazaki (2005), Possible effect of boreal wildfire soot on Arctic sea ice and Alaska glaciers, *Atmos. Environ.*, *39*(19), 3513–3520, doi:10.1016/j.atmosenv.2005.02.050.

LaChapelle, E. (1959), Annual mass and energy exchange on the Blue Glacier, *J. Geophys. Res.*, *64*(4), 443−449, doi:10.1029/JZ064i004p00443.

Lafon, S., J.-L. Rajot, S. C. Alfaro, and A. Gaudichet (2004), Quantification of iron oxides in desert aerosol, *Atmos. Environ.*, *38*(8), 1211–1218, doi:10.1016/j.atmosenv.2003.11.006.

Littell, J. S., M. Mcguire Elsner, L. C. Whitely Binder, and A. K. Snover (2009), The Washington Climate Change Impacts Assessment: Evaluating Washington's future in a changing climate—Executive Summary. *Rep.*, Univ. of Washington, Seattle, Wash.

McCabe, G. J., and A. G. Fountain (2013), Glacier variability in the conterminous United States during the twentieth century, *Clim. Change*, *116*(3–4), 565–577, doi:10.1007/s10584-012-0502-9.

Osterberg, E. C., M. J. Handley, S. Sneed, P. A. Mayewski, and K. J. Kreutz (2006), Continuous ice core melter system with discrete sampling for major ion, trace element, and stable isotope analyses, *Environ. Sci. Technol.*, *40*(10), 3355–3361.

Painter, T. H., N. Molotch, M. P. Cassidy, M. G. Flanner, and K. Steffen (2007), Contact spectroscopy for the determination of stratigraphy of snow grain size, *J. Glaciol.*, *53*, 121–127.

Painter, T., M. G. Flanner, G. Kaser, B. Marzeion, R. A. VanCuren, and W. Abdalati (2013a), End of the Little Ice Age in the Alps forced by industrial black carbon, *Proc. Natl. Acad. Sci. U.S.A.*, *110*(38), 15,216–15,221, doi:10.1073/pnas.1302570110.

Painter, T. H., F. C. Seidel, A. C. Bryant, S. McKenzie Skiles, and K. Rittger (2013b), Imaging spectroscopy of albedo and radiative forcing by light-absorbing impurities in mountain snow, *J. Geophys. Res. Atmos*, *118*, 9511−9523, doi:10.1002/jgrd.50520.

Rasmussen, L. A., H. Conway, and P. S. Hayes (2000), The accumulation regime of Blue Glacier, USA, 1914–96, *J. Glaciol.*, *46*(153), 326–334, doi:10.3189/172756500781832846.

Rhodes, J., R. L. Armstrong, and S. Warren (1987), Mode of formation of "ablation hollows" controlled by dirt content of snow, *J. Glaciol.*, *33*(114), 135–139.

Ricchiazzi, P., S. R. Yang, C. Gautier, and D. Sowle (1998), SBDART: A research and teaching software tool for plane-parallel radiative transfer in the Earth's atmosphere, *Bull. Am. Meteorol. Soc.*, *79*(10), 2101–2114, doi:10.1175/1520-0477(1998)079<2101:sarats>2.0.co;2.

Riedel, J., and M. A. Larrabee (2011), North Cascades National Park Complex glacier mass balance monitoring annual report, water year 2009: North Coast and Cascades Network *Rep.*, National Park Service, Fort Collins, Colo.

Schwarz, J. P., et al. (2006), Single-particle measurements of midlatitude black carbon and light-scattering aerosols from the boundary layer to the lower stratosphere, *J. Geophys. Res.*, *111*, D1607, doi:10.1029/2006JD007076.

Schwarz, J. P., R. S. Gao, A. E. Perring, J. R. Spackman, and D. W. Fahey (2013), Black carbon aerosol size in snow, *Nat. Sci. Rep.*, *3*, 1356–1460, doi:10.1038/srep01356.

Skiles, S. M. (2014), Dust and black carbon radiative forcing controls on snowmelt in the Colorado River Basin, dissertation thesis, Univ. of Calif., Los Angeles.

Skiles, S. M., T. Painter, J. Deems, A. Bryant, and C. Landry (2012), Dust radiative forcing in snow of the Upper Colorado River Basin: 2. Interannual variability in radiative forcing and snowmelt rates, *Water Resour. Res.*, *48*, W07522, doi:10.1029/2012WR011986.

Sokolik, I. N., and O. B. Toon (1999), Incorporation of mineralogical composition into models of the radiative properties of mineral aerosol from UV to IR wavelengths, *J. Geophys. Res.*, *104*(D8), 9423−9444, doi:10.1029/1998JD200048.

Takeuchi, N. (2002), Optical characteristics of cryoconite (surface dust) on glaciers: The relationship between light absorbency and the property of organic matter contained in the cryoconite, *Ann. Glaciol.*, *34*, 409–414.

Takeuchi, N. (2009), Temporal and spatial variations in spectral reflectance and characteristics of surface dust on Gulkana Glacier, Alaska Range, *J. Glaciol.*, *55*(192), 701–709.

Tegen, I., M. Werner, S. P. Harrison, and K. E. Kohfeld (2004), Relative importance of climate and land use in determining present and future global soil dust emission, *Geophys. Res. Lett.*, *31*, L05105, doi:10.1029/2003GL019216.

Toon, O. B., C. P. McKay, T. P. Ackerman, and K. Santhanam (1989), Rapid calculation of radiative heating rates and photodissociation rates in inhomogeneous multiple scattering atmospheres, *J. Geophys. Res.*, *94*(D13), 16,287–216,301, doi:10.1029/JD094iD13p16287.

Waddington, E. D., and R. T. Marriot (1986), Ice divide migration at Blue Glacier USA, *Ann. Glaciol.*, *8*, 175–176.

Ware, R. H., D. W. Fulker, S. A. Stein, D. N. Anderson, S. K. Avery, R. D. Clark, K. K. Droegemeier, J. P. Kuettner, J. B. Minster, and S. Sorooshian (2000), SuomiNet: A real-time national GPS network for atmospheric research and education, *Bull. Am. Meteorol. Soc.*, *81*(4), 677–694, doi:10.1175/1520-0477(2000)081<0677:SARNGN>2.3.CO;2.

Warren, S., and W. Wiscombe (1980), A model for the spectral albedo of snow II. Snow containing atmospheric aerosols, *J. Atmos. Sci.*, *37*, 2734–2745.

Wendel, R., and D. Zabowskl (2009), Fire history within the lower Elwha River watershed, Olympic National Park, Washington, *Northwest Sci.*, *84*(1), 88–97, doi:10.3955/046.084.0109.

Wendl, I. A., J. A. Menking, R. Farber, M. Gysel, S. D. Kaspari, M. J. G. Laborde, and M. Schwikowski (2014), Optimized method for black carbon analysis in ice and snow using the single particle soot photometer, *Atmos. Meas. Tech.*, *7*(8), 2667–2681, doi:10.5194/amt-7-2667-2014.

Westerling, A. L., H. G. Hidalgo, D. R. Cayan, and T. W. Swetnam (2006), Warming and earlier spring increase western US forest wildfire activity, *Science*, *313*(5789), 940–943, doi:10.1126/science.1128834.

Whicker, J. J., J. E. Pinder, and D. D. Breshears (2006), Increased wind erosion from forest wildfire: Implications for contaminant-related risks, *J. Environ. Qual.*, *35*, 468–578.

Wiscombe, W., and S. Warren (1980), A model for the spectral albedo of snow. I: Pure snow, *J. Atmos. Sci.*, *37*, 2712–2733.

Xu, B., J. Cao, D. Joswiak, X. Liu, H. Zhao, and J. He (2012), Post-depositional enrichment of black soot in snow-pack and accelerated melting of Tibetan glaciers, *Environ. Res. Lett.*, *7*(1), 014022, doi:10.1088/1748-9326/7/1/014022.

Yue, X., L. J. Mickley, J. A. Logan, and J. O. Kaplan (2013), Ensemble projections of wildfire activity and carbonaceous aerosol concentrations over the western United States in the mid-21st century, *Atmos. Environ.*, *77*, 767–780, doi:10.1016/j.atmosenv.2013.06.003.